論文 / 著書情報
Article / Book Information

Title	Centrifuge testing to investigate effects of partial saturation on the response of shallow foundation in liquefiable ground under strong sequential ground motions
Authors	Ritesh Kumar, Kazuki Horikoshi, Akihiro Takahashi
Citation	Soil Dynamics and Earthquake Engineering, Vol. 125, 105728
Pub. date	2019, 10
DOI	http://dx.doi.org/10.1016/j.soildyn.2019.105728
Creative Commons	See next page.
Note	This file is author (final) version.

License

Title:

Centrifuge testing to investigate effects of partial saturation on the response of shallow foundation in liquefiable ground under strong sequential ground motions

Authors:

Ritesh Kumar [a], Kazuki Horikoshi [b], and Akihiro Takahashi [c*]

[a] Graduate Student
Department of Civil and Environmental Engineering
Tokyo Institute of Technology
Email: kumar.r.aa@m.titech.ac.jp

[b] Assistant Professor
Department of Civil and Environmental Engineering
Tokyo Institute of Technology
Email: horikoshi.k.aa@m.titech.ac.jp

[c] Professor ([*]Corresponding author)
Department of Civil and Environmental Engineering,
Tokyo Institute of Technology
2-12-1-M1-3 Oh-okayama, Meguro, Tokyo 152-8552, Japan
Tel: +81-(0)3-5734-2593 Fax: +81-(0)3-5734-3577
Email: takahashi.a.al@m.titech.ac.jp

Soil Dynamics and Earthquake Engineering, 125, 105728, 2019

Official URL:

https://doi.org/10.1016/j.soildyn.2019.105728

Abstract

Induced partial saturation is one of the novel techniques to increase the liquefaction resistance of saturated sandy ground. Nonetheless, a limited number of experimental studies are available on the delineation of this method. Moreover, the performance of induced partial saturation under sequential ground motions is poorly understood. Dynamic centrifuge experiments are carried out to investigate the effects of partial saturation on the response of shallow foundation resting on liquefiable ground under sequential ground motions. Centrifuge models consist of two distinct shallow foundations and associated superstructures resting on a liquefiable uniform sand layer. The drainage-recharge method is used to induce partial saturation in the model ground. Compressibility change of pore fluid and alteration of ground permeability because of induced air voids, affect the deformation mechanism of the ground-foundation system. Assessment of maximum potential volumetric compressibility of pore fluid because of induced air voids is essential to understand the effectiveness of induced partial saturation. Centrifuge test results signify that the induced partial saturation reduces the overall deformation of the foundation-structure system. However, slightly amplified kinematic seismic demand is observed at superstructures in case of partially saturated ground in comparison with fully saturated ground.

Keywords

Centrifuge model test, excess pore water pressure, induced partial saturation, liquefaction, sequential ground motion, settlement, shallow foundation

1. Introduction

Liquefaction, a well-known phenomenon has been a topic of curiosity and complex experimentation among the geotechnical earthquake engineers and researchers all over the world since the past few decades. Liquefaction primarily occurs in the saturated loose cohesionless soil during dynamic/cyclic loading. During liquefaction, soil loses its shear strength due to excessive build-up of pore water pressure leading to ground failure, and sometimes even collapse of associated structures. Soil liquefaction and related ground failure have been extensively studied by many researchers [1-7]. Liquefaction has caused damage to the built environment to a great extent. For instance, a significant part of the Christchurch city in New Zealand was devastated by soil liquefaction during the 2011 Christchurch earthquake in terms of the structural settlement, tilting, and lateral spreading of the ground [6, 7]. In the 1964 Niigata and the1990 Luzon (Philippines) earthquakes, most of the damaged buildings were two to four stories built on shallow foundations and relatively thick and uniform deposits of clean sand. Reports presented in many studies [8-10] described the role of liquefaction in the damage of buildings, specifically in the reclaimed land during the 2011 Tohoku earthquake. Numerous sand boils and large ground settlement, as well as the settlement/tilting of the wooden houses and reinforced concrete buildings supported on spread foundation, were seen throughout the affected area.

Soil remediation measures are requisite for liquefaction prone sites. In recent years, many researchers have explored liquefaction mitigation techniques that are different from commonly available practices as presented in reports by Mitchell et al., and Seed et al. [11-13]. Among those newly developed methods, induced partial saturation is one of the novel techniques to increase the liquefaction resistance of liquefiable ground. Partial saturation is achieved by artificially introducing the gas bubbles into soils. Several methods have been adopted to induce partial saturation within the ground such as water electrolysis [14], drainage-recharge [14, 15], chemical sodium perborate [16], biogas [17] and air injection [18, 19].

Laboratory experiments were performed by many researchers [20, 21] to understand the performance of induced partial saturation. The results showed that even a small change in the degree of saturation could increase the liquefaction resistance of liquefiable soil considerably. The inclusion of air voids within the saturated ground (to make it partially saturated) tend to decrease the overall bulk modulus and increase the compressibility of the pore fluid, which makes the development of excess pore water pressure less under cyclic shearing compared to the fully saturated condition. In this study, the drainage-recharge method is used to induce the partial saturation within the ground.

A comprehensive investigation is required to understand the effectiveness of induced partial saturation to mitigate the liquefaction effects on a shallow foundation. The effectiveness of air voids under multiple shaking, partial drainage effects on the evolution of excess pore water pressure, post-liquefaction behavior and soil-foundation-structure inertial and kinematic interaction are essential to assimilate to avail the maximum benefits of this technique. For that purpose, two dynamic centrifuge experiments are carried out to examine the performance of induced partial saturation to mitigate the liquefaction effects on shallow foundation under strong sequential ground motions.

2. Centrifuge Test Program

Dynamic centrifuge tests are performed to investigate the effectiveness of induced partial saturation to mitigate the liquefaction effects on a shallow foundation. Dynamic centrifuge tests are carried out utilizing the Tokyo Tech Mark III centrifuge facility [22] having a radius of 2.45 m, at a centrifugal acceleration of 40 g (*N=40*). Presented centrifuge tests simulate the prototype saturated soil deposit of 10 m depth. The model ground is prepared using the Toyoura sand (properties are shown in Table 1) with a relative density; of 50% by the air-pluviation method. The sand hopper is precisely calibrated in terms of the falling height and pouring rate to ensure the consistency of relative density for different model grounds. A flexible laminar container with inner dimensions of 600 x 250 x 438 mm (model scale) in length, width, and height respectively, is used to frame the models. The laminar box is

composed of many aluminum rectangular alloy rings which allow the movement along with soil mass which helps to create a flexible boundary and ensure the uniform dynamic shear stresses within the model ground during the dynamic excitation.

2.1 Model foundation-structure system

The scope of this paper is to evaluate the effectiveness of induced partial saturation for the isolated shallow foundation associated with temporary kind of structures resting on liquefiable ground. Therefore, two different types of superstructures (as shown in Fig. 1) are considered, in which left unit represents a typical Buffer Tank (BT), and right unit represents Flare Stack (FS). BT and FS (properties are shown in Table 2) impose an average bearing pressure of 51.2 kPa and 71.2 kPa respectively at 0.8 m below the surface of the model ground in prototype scale as shown in Fig. 1. BT is a kind of storage tank, and FS is typically used to burn the unusable waste. They are generally mounted on an isolated shallow foundation. These two different structures are used to understand the rocking behavior (anticipated for FS as being the taller structure) of the structures during the shaking. Also, the effectiveness of induced air-voids is investigated under different bearing pressure with the help of BT and FS foundation-structure system. Moreover, the use of two different structures ensured the credibility of the evaluated performance of induced partial saturation. The height of prototype targeted structures, i.e. BT and FS are 15 m and 32 m respectively, having distributed mass along the height. In the model scale, the height of both BT and FS (after scaling down for $N = 40$) turned out quite disproportionate concerning the laminar container size. Therefore masses are lumped at the middle of both BT and FS to ensure the fundamental design periods of BT and FS (0.4s and 0.5s, respectively). This improvisation reduced the height of BT and FS by 50.10% and 56.25 % respectively.

2.2 Model ground preparation

Flow charts of model ground preparation for both fully saturated and partially saturated model grounds

123 are shown in Fig. 2. Initially, the water tightness is ensured to avoid any fluid leakage from the laminar
124 container during the experiment. Inner sides of the laminar box are covered with the polyethylene sheet
125 to prevent any sand particles jamming between the alloy rings. Then sand is poured with the help of a
126 sand hopper which is manually moved forth and back to achieve the uniform level ground at calibrated
127 falling height and pouring rate. The transducers are carefully placed at desirable locations (see Fig.1
128 and Table 3) during the model ground preparation. The model is saturated with the viscous fluid, i.e.,
129 a mixture of water and 2 % Metolose (Hydroxypropylmethyl cellulose) by weight of water, to achieve
130 a viscosity about 40 times that of water. This solution is used to ensure the compatibility of prototype
131 permeability of the soil and to set up the affinity between dynamic and diffusion scaling laws [23]. The
132 fully saturated model ground is prepared by dripping the de-aired Metolose solution slowly from the
133 top of the container under a vacuum of 760 mmHg over the sponges at the surface of the model ground.
134 The dripped solution slowly moves downward and saturates the model ground uniformly. The
135 saturation is continued until the water table (Metolose solution table) reaches up to the top surface of
136 the model ground. This saturation process for both the models took approximately 48 hours to complete.
137 After the saturation, superstructures (BT and FS) are mounted over the footings and placed on the
138 model ground at desirable locations (as shown in Fig. 1). It is to be noted that the wind speed at 40 g
139 is tremendous which might cause turbulence to the FS because of comparatively large height.
140 Therefore a wind casing is prepared to cover it as shown in Fig. 3.
141
142 *2.3 Air induction*
143 The drainage-recharge method is used to prepare the partially saturated model ground. Initially, the
144 model ground is prepared and saturated as described in the Subsection mentioned above. After the
145 saturation, the laminar box is taken out from the vacuum chamber. Then, the partial saturation is
146 induced at 1g as follows (Fig. 2): In the first step, the Metolose solution is drained out from the model
147 ground which turns the model into moist state and entrapped some amount of the air voids inside it. In

step 2, the drained-out Metolose solution is dripped back slowly on the sponges at the surface of the model ground in open air. The recharging is continued until the water table reaches back to the top surface of the model ground. It is to be noted that this time some amount of Metolose solution is left out because of entrapped air even though the water table reaches up to the top surface. The process mentioned in step 2 is repeated three times to ensure the uniformity of air voids entrapped within the model ground. Each time it took almost 4 hours to complete the drainage-recharge cycle. The overall degree of saturation within the partially saturated model ground is estimated by W_2/W_1, where W_2 and W_1 are the amounts of Metolose solution used in preparing the partially saturated and fully saturated model ground respectively. Due care is taken to estimate the degree of saturation for both fully saturated and partially saturated model grounds (tabulated in Table 4) using mass, volume and density relationships. However, it is worth noting that certain errors still happen to have a scope as mentioned by Kutter [24].

2.4 Water table and effective stress

The location of the water table is estimated using pore pressure readings of many pore pressure transducers at 40g to avoid/minimize any possible error. Estimated water tables for fully saturated and partially saturated model grounds are found to be at 0.7 m and 0.9 m respectively, below the surface of the ground in prototype scale. The vertical effective stress is one of the fundamental factors which determines the soil behavior. All measurable effects of change of stress, such as compression, distortion and a change of shearing resistance, are due exclusively to changes of effective stress [25]. The initial effective stress is calculated (as tabulated in Table 3) by subtracting the pore water pressure from the total stress. Vertical stress at desirable depths because of foundation-structure is calculated using Boussinesq's method which further is used to evaluate the vertical effective stress distribution within the ground.

2.5 Testing procedure

After finishing the saturation process, the model is mounted on the shaking table at centrifuge lab facility. Before applying the ground motions, the centrifuge model is tested against a white noise (WN1) as shown in Fig. 4 to understand the dynamic characteristics of the system. Fig. 5 shows the transfer function which is estimated as the ratio of acceleration obtained at the top of superstructures (A8 and A9 as shown in Fig. 1) to the white noise acceleration recorded at the base of the centrifuge model ground (A1) in the frequency domain. The fundamental periods obtained during the experiments are 0.42 and 0.37 s for BT, and 0.56 and 0.58 s for FS corresponding, respectively, for fully saturated and partially saturated model grounds in prototype scale. Natural periods of BT and FS obtained for both the models are very close to the design periods (as mentioned in Table 2). Ground motion recorded at Hachinohe Port during the 1968 Tokachi-Oki earthquake (NS component) is used as the first dynamic excitation after the white noise (WN 1). Enough time is given for full dissipation of excess pore water pressure before applying the second/sequential earthquake ground motion. Design earthquake motion for highway bridges in Japan (2-I-I-3, NS component) recorded at the ground surface near New Bansuikyo Bridge, Tochigi during the 2011 Tohoku Earthquake is used as the sequential ground motion to examine the foundation behavior under large earthquake. Model grounds configuration and the description of applied shakings are tabulated in Table 4. Fig. 6 shows the acceleration time histories, Fourier spectra and Arias intensity [26] of the input base motions for fully saturated and partially saturated model grounds. Exact simulation of ground motion in the centrifuge is quite complicated. Many trials were made to finalize the simulated shakings (of both Tokachi-Oki and Tohoku ground motions) before performing the centrifuge experiment. It is imperative that the simulated ground motions agree well in time and frequency domain as well as depict alike Arias intensity to ensure the fair comparison between test results of fully and partially saturated model grounds. Base motions shown here are presented after having baseline correction and filtering. Filtering is performed in the frequency domain using the bandpass Butterworth filter with corner

198 frequencies of 0.3Hz and 10 Hz respectively in prototype scale. It is evident that the simulated
199 waveforms for both cases possesses similar intensity and are in good agreement both in time as well
200 as frequency domain.
201
202 **3. Test Results and Discussion**
203 *3.1 Evolution of excess pore water pressure*
204 All the test results shown in the following sections are in the prototype scale unless mentioned
205 otherwise. Excess pore water pressure (EPWP) time histories are obtained at several desirable locations
206 as shown in Fig. 1. Evolution of EPWP (generation and dissipation trend), plays a vital role in the
207 understanding of the liquefaction phenomena. Soils at certain depth undergo liquefaction if the excess
208 pore water pressure ratio (r_u) which is calculated by dividing the generated EPWP by the initial vertical
209 effective stress at the respective depth, approaches to unity. Table 3 shows the initial vertical effective
210 stress at all transducers locations for both fully saturated and partially saturated model grounds.
211 Fig. 7 depicts the EPWP time histories for the fully saturated and partially saturated model grounds
212 when subjected to Tokachi-Oki ground motion. At P1 (Level 1), the EPWP time histories are almost
213 same in both the cases in terms of maximum magnitude; though, the dissipation trend is marginally
214 delayed in case of partially saturated model ground. As the hydrostatic pressure at Level 1 (base of the
215 model ground) is significantly high, there might be a possibility of volume change/dissolution of air
216 voids. Therefore, both fully saturated and partially saturated model grounds exhibit similar behavior
217 in terms of generated EPWP trends at the base of the model ground which is further elaborated in the
218 following Subsection. At P2 and P4 (Level 3), the presence of air voids within the partially saturated
219 model ground significantly delayed the generation and dissipation of EPWP in comparison with the
220 fully saturated model ground. This behavior occurs primarily because of the increase in compressibility
221 of the air and pore fluid mixture in case of partially saturated model ground [14]. In addition, induced
222 partial saturation reduced the overall permeability of partially saturated ground. This also justifies the

behavior of the slower rate of generation and dissipation of EPWP as shown in Fig. 7. At this level (Level 3), the maximum magnitude of generated EPWP has surpassed the liquefaction state line (i.e. r_u=1) in case of fully saturated model ground whereas the liquefaction state is not observed in case of the partially saturated model ground. Similar behavior of EPWP generation and dissipation is observed at P6 (Level 4). In case of fully saturated model ground, liquefaction state is achieved at P6 whereas, the maximum magnitude of EPWP in case of the partially saturated model ground is far below the liquefaction state line. Unfortunately, the pore water pressure transducers P3 and P5 did not work correctly because of some unforeseen reasons and hence are not shown in Fig. 7.

At shallower depth (Level 5), EPWP time histories at P7 share almost the same magnitude of maximum EPWP for both fully saturated and partially saturated model grounds. However, the generation and dissipation rate of EPWP at P7 is delayed in case of partially saturated model ground in comparison with the fully saturated model ground. The possible explanation for this unusual behavior at P7 might be non-uniformity of partial saturation in the vicinity of Flare Stack (FS) footing. At P9 (Level 5), the maximum magnitude of generated EPWP is significantly less in case of partially saturated model ground in comparison with the fully saturated model ground. The liquefaction state is not achieved at P7 (under FS) and P9 (under BT) because of large vertical effective stress due to the foundation-structure system. It is interesting to note that the maximum magnitude of EPWP at P8 (Level 5) in case of the fully saturated model ground is more than the one at P7 and P9, even though the vertical stress at P8 is less than P7 and P9. The reason for this is the flow of pore fluid and settlement caused under the shallow foundation [13, 27]. Both BT and FS foundation has influence zone of large confining stress in the vicinity of foundation, and because of vertical hydraulic gradient setup during dynamic excitation, the pore fluid is bound to flow nearby the model centerline. The availability of significant amount of migrated pore fluid for a long time resulted in more EPWP at P8 than P7 and P9.

Fig. 8 depicts the EPWP time histories for both fully saturated and partially saturated model grounds when subjected to Tohoku ground motion. It is evident from Fig. 8 that whole model ground gets

liquefied except in the vicinity of FS foundation (at P7) in case of fully saturated model ground. However, induced partial saturation can avoid the liquefaction state at P6 (Level 4) and P7 and P9 (Level 5) in case of the partially saturated model ground. During Tohoku ground motion, the overall performance of partially saturated ground is diminished in comparison with the one witnessed during Tokachi-Oki ground motion. Tohoku earthquake is stronger than the Tokachi-Oki in terms of both peak acceleration and duration. Also, there is a considerable possibility that a few percentages of air voids might have disintegrated/dissolved during Tokachi-Oki earthquake because of pore fluid migration in the liquefied zone (further elaborated in Subsection 3.2) and due to the deformation of the model ground.

Pore pressure transducers (PPTs) at a shallower depth (P7-P9) exhibit maximum EPWP quite after the shaking period in case of partially saturated model ground during both Tokachi-Oki and Tohoku ground motion as shown in Figs 7-8. The reason for this is the slower rate of water flow from the deeper portion of the model ground in case of partially saturated ground. It is to be noted that all PPTs show a small magnitude of the residual EPWP in dissipation phase at 5000 s except at P1 (Figs. 7-8). This is associated with the fact that the PPTs experienced a marginal settlement during the shakings which changed the overall void ratio (probably decreased) and the marginal rise of the water table. This inevitable settlement of PPTs during Tokachi-Oki ground motion changed the initial vertical effective stress condition at the location of PPTs for Tohoku ground motions. However, the initial vertical effective stress is assumed to be constant for both the ground motions (Tokachi-Oki and Tohoku earthquake) at different levels in the model ground as mentioned in Table 3 for the sake of brevity.

3.2 Air void dissolution/collapse during shaking

Air voids are introduced using the drainage-recharge method to induce partial saturation within the model ground in this study. The detailed process of air induction is already described in Subsection 2.3. It is to be noted that the model grounds are prepared in 1g condition and the calculated degree of

saturation is certain to change at 40g environment within the partially saturated model ground. Introducing Boyle's law and assuming air voids to be isolated and soil grains to be incompressible, the distribution of the degree of saturation is estimated within the partially saturated model ground at 40g. Fig. 9 depicts that the degree of saturation increases (significantly) at the deeper portion of the model ground due to high hydrostatic pressure condition. This is also confirmed by the evolution of excess pore water pressure (EPWP) as explained in the previous Subsection. There are two governing factors by which the induced partial saturation can increase the liquefaction resistance of the ground. The first factor is the increase in the compressibility of the pore fluid due to the air voids entrapped within the pore fluid. This mechanism helps to restrict the rate of development of excess pore water pressure during cyclic loading which is also witnessed during the EPWP build-up stage in the experiment as depicted from Figs.7-8. The second one is matric suction which is not significant in the case of liquefiable soil as explained by Bishop and Blight [28]. By implementing the above stated Boyle's law, the maximum potential volumetric compressibility (strain) within the model ground can be estimated using the evolution of EPWP during the shaking [21, 29]. Consider a fully saturated soil mass comprising incompressible soil particles and pore fluid. For a small change in pressure, the volumetric strain in soil mass will be zero under undrained condition. However, the soil mass with air voids (partially saturated case) will undergo considerable volumetric strain (potential volume compressibility) under the same conditions. This potential volume compressibility of soil mass is solely due to the inclusion of air voids as the water and sand particles are assumed to be incompressible. The empirical equation proposed by Okamura and Soga [21] is used to estimate the potential volumetric compressibility which required the parameters such as the degree of saturation (Fig. 9), initial vertical effective stress (Table 3), maximum excess pore water pressure, and the initial void ratio (Table 1).

Fig. 10 shows the maximum potential volume compressibility because of air voids induced within the partially saturated model ground during white noise 1 (WN1, before Tokachi-Oki ground motion) and

white noise 2 (WN2, after Tohoku ground motion). The maximum potential volumetric strain depends on several factors such as void ratio, the evolution of EPWP, dynamic shaking, vertical effective stress and degree of saturation. Considering these factors and to evaluate the available potential volumetric compressibility before and after the main shakings, four locations (at P2, P4, P5, and P6 as shown in Fig.1) are considered during the white noises. The reason for selecting pore pressure locations at Levels 3 and 4 (at P2, P4, P5, and P6) is to avoid/minimize the influence of an abrupt change in void ratio and degree of saturation during and after the shaking. Both white noise shakings (WN1 and WN2) are alike as shown in Fig. 10 and possess almost same intensity. It is evident from Fig. 10 that the availability of maximum potential volumetric compressibility because of induced air voids during WN1 is relatively more than that available during WN2. This is associated with the fact of air void dissolution/collapse during Tokachi-Oki and Tohoku ground motion which is also witnessed from the EPWP time histories (Fig. 8) as explained in the previous Subsection. However, the available capacity of potential volume compressibility is quite significant even after the strong Tohoku ground motion (corresponds to WN2) which signifies the novelty of induced partial saturation to increase the liquefaction resistance of the partially saturated ground.

3.3 Permeability of partially saturated ground

Fig. 11 shows the soil-water characteristic curve for Toyoura sand [30]. The permeability of partially saturated model ground at a different degree of saturation (along the depth as shown in Fig. 9) is estimated using van Genuchten model [31]. Initially, the van Genuchten model parameters for Toyoura sand are calculated using the experiment data retrieved from Unno et al. [30]. Then, the variation of the degree of saturation along the depth of the partially saturated model ground (Fig. 9) is used to estimate the volumetric water content. After that, the effective degree of saturation S_e [31] is determined and used to calculate the permeability coefficient. The permeability coefficient plotted in Fig. 12 is the ratio of K_{P_sat} (permeability of partially saturated ground) and K_{F_sat} (permeability of fully

saturated ground). For detail procedure of permeability estimation, readers are suggested to refer Unno et al. [30] and Fredlund et al. [32]. It is evident from Fig. 12 that the permeability within the partially saturated model ground reduced significantly as much as up to 40 % to 60 % of the permeability of fully saturated model ground. 1-D consolidation analysis is also performed to estimate the overall relative permeability of the partially saturated ground. With appropriate boundary conditions and an initial value of pore water pressure at the end of the shaking (or at the beginning of dissipation phase), the dissipation curve of pore water pressure is estimated at P2 and P4 for both fully saturated and partially saturated grounds during Tokachi-Oki ground motion. The dissipation phase of pore water pressure is governed by the coefficient of consolidation which includes soil permeability, compressibility, and unit weight of pore fluid. The estimated dissipation curves of pore water pressure at P2 and P4 are fitted with the centrifuge test results by changing the permeability values [33]. Then the average permeability coefficient (K_{P_sat}/ K_{F_sat}) for P2 and P4 is obtained which is found to be 0.73 during the Tokachi-Oki ground motion. This also corroborates the fact that induced air-voids reduce the overall permeability of the partially saturated ground.

3.4 Settlement behavior

Fig. 13 depicts the settlement observed at BT and FS footings during Tokachi-Oki ground motion. Two laser displacement transducers (LDTs) are used to record the footing settlement for BT (LDTs 1, and 2) and FS (LDTs 3, and 4). It is evident that both BT and FS footings undergo excessive settlement in case of fully saturated ground. The foundations begin to settle immediately after the shaking began and continued even after the shaking ceased. BT footing exhibits large magnitude of differential settlement (the difference between the settlements of both sides of the footing) by the side of LDT1 in case of the fully saturated ground; whereas, FS footing exhibits comparatively smaller but significant magnitude of differential settlement in case of partially saturated ground. Seismic demand, relative density, liquefaction state, foundation height/width ratio, bearing pressure and overall drainage in the

vicinity of the foundation are few of the factors to mention which govern the overall liquefaction induced settlement mechanism of shallow foundation [27]. In addition, the non-uniform degree of partial saturation in the ground might be responsible for the differential settlement of foundation-structure system in case of partially saturated ground. A sudden jump in LDT2 reading (see * in Fig. 13) in the very beginning of shaking is apparent which might be because of movement of the sensor holder/plate as such sudden change could not be seen in all other sensors.

Fig. 14 depicts the settlement observed at BT and FS footing during Tohoku ground motion. In case of fully saturated ground, both BT and FS experienced collapse kind of behavior (from the visual inspection after the experiment, it is found that both BT and FS had struck to the surrounding guide plate). As explained earlier, during Tokachi-Oki ground motion, BT footing exhibits the significant amount of differential settlement in the direction of LDT1 in case of fully saturated ground. The rotational tilting (as it seems to have happened from Fig. 14) occurred after the Tohoku ground motion, and BT footing concludes with excessive differential settlement by the side of LDT2. This unusual behavior of BT during Tohoku ground motion in case of fully saturated model ground might have happened because of the soil flow (traces were observed after the experiment) over the location of LDTs 1, 2 and 4 during Tohoku ground motion because of liquefaction. In that case, the LDTs (1, 2 and 4) readings, especially after the soil overflow (dashed lines in Fig. 14), are not reliable in case of fully saturated model ground for Tohoku ground motion. It is evident from Figs. 13-14, that the overall performance of the partially saturated ground for both the footings and associated superstructures is better than the fully saturated ground.

Fig. 15 shows the cumulative average settlement of BT and FS footings during and after the shakings (Tokachi-Oki and Tohoku ground motions). It is evident that footings undergo significant co-shaking settlement (settlement occurred during shaking) in case of fully saturated model ground during both Tokachi-Oki and Tohoku ground motion. Shear-induced deformation is the governing factor for co-shaking settlement, and it can be seen from Fig. 15 as the overall vertical settlement of FS is

significantly large compared to the vertical settlement of BT. The shear strength of soil in the vicinity of the foundation start to mobilize because of generation of excess pore water pressure (reduction in mean vertical effective stress) and hence shear-induced co-shaking settlement is apparent. The induced partial saturation can mitigate the shear-induced deformation as the co-shaking settlement in case of the partially saturated ground is less in comparison with the fully saturated ground. Volumetric strains due to partial drainage and development of post-liquefaction/shaking reconsolidation strains are the prime responsible factors associated with the post-shaking settlement. It is evident from Fig. 15 that the post-shaking settlement is significantly mitigated by the presence of air voids in case of partially saturated model ground. Unfortunately, the post-shaking readings of LDTs in case of fully saturated ground are not reliable during Tohoku ground motion as discussed earlier and hence are not shown in Fig. 15. Fig. 16 depicts the surface settlement (topography) measured after the centrifuge experiments. The surface settlement is shown in Fig. 16 is the cumulative response during all the shakings. Larger the bearing pressure more is the settlement in the vicinity of the foundation for both fully saturated and partially saturated ground. It is evident that the overall surface settlement is significantly less in case of partially saturated ground in comparison with fully saturated ground.

3.5 Kinematic and inertial interaction between the model ground-foundation-structure system

It is a well-established fact that during the dynamic excitation soils undergo deformations which are further foisted on the foundation. During the seismic loading, the wave propagates through the soil media which altered in the vicinity of the structure. This well-known phenomenon of soil-structure interaction dominatingly governs the structure behavior in the liquefiable ground. Inertial interaction is not significant in case of liquefiable ground because the soil is assumed to behave as a seismic isolator to the foundation [34]. However, superstructure's dynamic properties that control inertial interaction (e.g., mass, stiffness, height to width ratio) have shown significant influence on the evolution of the pore water pressure, settlement trend, tilt potential, which in turn, affect the overall

performance of superstructure [35].

Fig. 17 depicts the acceleration time histories recorded at several locations on/within foundation-superstructure and model ground (see Fig. 1). The position of A5 (at Level 5) along the model centerline is considered as the far-field (FF). Although A5 is placed significantly away from, and approximately at the same level of the base of the footings of both structures, some interaction is still expected to happen due to spacing constraints between the structures. Acceleration records measured at A5 showed the significant amount of de-amplification in acceleration time histories for both fully saturated and partially saturated model grounds during Tokachi-Oki and Tohoku ground motions. Significant de-amplified acceleration time history of A5 also consolidate the fact that the model ground exhibits considerable softened state during Tokachi-Oki and Tohoku ground motions. Partially saturated ground shows relatively less de-amplification in comparison with the fully saturated ground at all locations except at A7 and A9 in case of Tohoku ground motion. This explains that the partially saturated model ground exhibits more liquefaction resistance (relatively less model ground softening) in comparison with the fully saturated model ground. Similar observations of acceleration records were made by Zeybek and Madabhushi [36]. During Tohoku ground motion, acceleration time histories recorded at the foundation and superstructure of FS (A7 and A9) showed the spikes in case of fully saturated ground. The reason for this might be the excessive settlement of the foundation [27]. Also, larger acceleration spikes at the FS might be observed because of soil dilation and re-stiffening caused by excessive soil flow under the shallow foundation.

To examine the influence of the kinematic and inertial interaction on foundation, Fourier amplitude spectra (FAS) of acceleration records at footings and far-field is obtained as shown in Fig. 18. The FAS representation of acceleration records can give an insight of amplification/attenuation between fully saturated and partially saturated ground at respective locations. The frequency content can be divided into two ranges; i.e., acceleration dominating (*Fa*) and velocity dominating (*Fv*) range as suggested by Borcherdt [37]. It is evident that the FAS amplitudes for FF and BT are significantly large in case of

423 partially saturated model ground in comparison with the fully saturated ground during both Tokachi-
424 Oki and Tohoku ground motions. The observed amplification is more dominating in the *Fv* frequency
425 (0.5–2.0 Hz) range. This demonstrates that the partially saturated ground yield amplified seismic
426 demand to the model ground-foundation system. However, the FAS trend for FS footing seems to be
427 alike for both fully saturated and partially saturated grounds during Tokachi-Oki ground motion.
428 Although, a marginal attenuation in FAS is observed for high frequency in case of partially saturated
429 ground. The reason for this is alike model ground condition in the vicinity of FS footing as the degree
430 of saturation is almost same for both fully saturated and partially saturated ground.
431
432 *3.6 Strength/Stiffness mobilization of model ground*
433 Fig. 19 depicts transfer functions (TFs) during white noise 1, Tokachi-Oki, and Tohoku ground motions.
434 The ratio of acceleration records at A5 to A1 in the frequency domain is used to obtain the TFs. It is
435 evident that the fundamental site frequency obtained for both fully saturated and partially saturated
436 grounds during white noise 1 falls within the range of small-strain site fundamental frequency obtained
437 by empirical equations [38], even though the soil response is highly nonlinear. This also implies that
438 the fundamental site frequency of the model ground could be captured by appropriate white noise
439 (usually a random small amplitude vibration having equal intensities at different frequencies, giving it
440 a constant power spectral density). Shear wave velocity profile (within the ground using small strain
441 shear pulse) is used in empirical equations to estimate the fundamental site frequency. The upper and
442 lower bound of the fundamental frequency of the model ground (2.5~2.8 Hz) is determined by the
443 estimated range of shear wave velocity (approximately 169 to 186 m/s) using empirical equations as
444 mentioned above. Site fundamental frequencies obtained during Tokachi-Oki ground motion falls to
445 0.54 and 0.8 Hz for the fully saturated and partially saturated model ground respectively. The
446 significant drop in site fundamental frequency occurred because of the softening of the model ground
447 during Tokachi-Oki ground motion [39]. It is evident that the extent of model ground softening is

448 relatively small in case of partially saturated ground in comparison with the fully saturated ground.
449 However, both the model grounds exhibit nearly same trend of TFs during Tohoku ground motion.
450 Back analysis of acceleration records, is performed to get the insight into the progression of shear
451 strain within the model ground. Many studies justify the credibility of this method. Zeghal et al. [40];
452 Adalier and Elgamal [41] used the recorded lateral accelerations to evaluate shear stress and strain
453 histories at different elevations within the ground. Brennan et al. [42] assessed the shear modulus and
454 shear degradation curves for dry and saturated sand, soft clay from the acceleration histories obtained
455 from the centrifuge tests. Fig. 20 depicts the shear strain developed along the centerline of the model
456 ground between different levels (as mentioned in Table 3) during the centrifuge test for fully saturated
457 and partially saturated grounds. At a shallower depth (between Levels 4 and 5), the shear strain
458 developed within the partially saturated ground is significantly less in comparison with fully saturated
459 ground. Similar behavior is observed between Levels 3 and 4. This behavior corroborates the fact that
460 inclusion of air voids within the ground increases the liquefaction resistance of the ground. However,
461 shear strain time histories between Levels 2-3 and Levels 1-2 are alike for both fully saturated and
462 partially saturated grounds. The presence of air voids seems to have negligible effects at the deeper
463 portion. Excess pore water pressure time histories obtained at the deeper portion (Figs. 7 and 8) also
464 delineate the limitation of the presence of the air voids under higher stress level.
465
466 **4. Conclusions**
467 Dynamic centrifuge experiments are carried out to investigate the effects of partial saturation on
468 shallow foundation resting on liquefiable ground under sequential ground motions. The drainage-
469 recharge method is used to induce partial saturation within the liquefiable ground. The response of
470 partially saturated ground is compared with the fully saturated ground in terms of the evolution of
471 excess pore water pressure at several locations, settlement time histories of footings, and kinematic
472 and inertial interaction between soil-foundation-structure system. The observed slower rate of

generation and dissipation of excess pore water pressure in case of partially saturated ground, consolidate the fact that the compressibility of pore fluid increases because of inclusion of the air voids within the ground. Also, the partially saturated ground shows overall less permeability in comparison with the fully saturated ground. Partially saturated ground exhibited a significant amount of maximum potential volumetric compressibility of pore fluid after the strong Tohoku ground motion (sequential motion applied after Tokachi-Oki ground motion) which justify the efficacy of induced partial saturation. In case of fully saturated ground, the foundation-structure systems undergo excessive settlement with complete bearing failure under the foundation during Tohoku ground motion. Whereas, induced partial saturation can minimize the settlement of foundation-structure systems in case of partially saturated ground. The kinematic seismic demand experienced by foundation-structure systems is relatively large in case of partially saturated ground in comparison with fully saturated ground. Despite that fact, centrifuge experiments show promising results in favor of induced partial saturation to mitigate the liquefaction-induced effects on shallow foundation.

Acknowledgments

The work presented in this paper is part of the collaborative research with the Nippon Steel & Sumikin Engineering. The authors would like to thank Dr Ece Eseller-Bayat, Istanbul Technical University, for useful discussions. Her visit to Tokyo Institute of Technology and the last author's visit to Istanbul Technical University were supported by Japan-Turkey Cooperative Education Program on Resilience Engineering for Energy and Urban Systems (funded by JSPS). The first author sincerely acknowledges the support provided by Monbukagakusho (Ministry of Education, Culture, Sports, Science, and Technology) scholarship for graduate students. The authors are also indebted to Mr. Sakae Seki, lab technician, Department of Civil and Environmental Engineering, Tokyo Institute of Technology for his tremendous contribution in the successful completion of centrifuge experiments.

Reference

[1]. Seed RB, Dickenson SE, Riemer MF, Bray JD, Sitar N, Mitchell JK, Idriss IM, Kayen RE, Kropp A, Hander Jr. LF, Power MS. Preliminary report on the principal geotechnical aspects of the October 17, 1989, Loma Prieta Earthquake. Rep. No. UCB/EERC-90/05, Earthquake Engineering Research Center, Uni. of California, Berkeley, 1990.

[2]. Ishihara K, Haeri SM, Moinfar AA, Towhata I, Tsujino S. Geotechnical aspects of the June 20, 1990 Manjil Earthquake in Iran. Soils and Foundations 1992; 32(3):61–78. https://doi.org/10.3208/sandf1972.32.3_61.

[3]. Bardet JP, Oka F, Sugito M, Yashima A. The Great Hanshin Earthquake disaster. Preliminary Investigation Rep., Dept. of Civil Engineering Univ. of Southern California, Los Angeles, 1995.

[4]. Sugito M, Oka F, Yashima A, Furumoto Y, Yamada K. Time-dependent ground motion amplification characteristics at reclaimed land after the 1995 Hyogoken Nambu Earthquake. Engineering Geology 2000; 56(1):137–150. https://doi.org/10.1016/S0013-7952(99)00139-8.

[5]. Krinitzsky EL, Hynes ME. The Bhuj, India, earthquake: lessons learned for earthquake safety of dams on alluvium. Engineering Geology 2002; 66(3):163–196. https://doi.org/10.1016/S0013-7952(02)00049-2.

[6]. Green RA, Cubrinovski M, Wotherspoon L, Allen J, Bradley B, Bradshaw A. Geotechnical reconnaissance of the 2011 Christchurch, New Zealand earthquake. Geotechnical Extreme Events Reconnaissance (GEER) Report 2011; 1(8).

[7]. Cubrinovski M, McCahon I. Short term recovery project 7, CBD foundation damage. Natural Hazards Research Platform. Christchurch, New Zealand, University of Canterbury, 2012.

[8]. Nakai S, Sekiguchi T. Damage due to liquefaction during the 2011 Tohoku earthquake. In Proc. of the International Symposium for CSMID 2011; 1-8.

[9]. Bhattacharya S, Hyodo M, Goda K, Tazoh T, Taylor CA. Liquefaction of soil in the Tokyo Bay area from the 2011 Tohoku (Japan) earthquake. Soil Dynamics and Earthquake Engineering

2011; 31(11):1618-1628. https://doi.org/10.1016/j.soildyn.2011.06.006.

[10]. Tokimatsu K, Tamura S, Suzuki H, Katsumata K. Building damage associated with geotechnical problems in the 2011 Tohoku Pacific Earthquake. Soils and Foundations 2012;52(5): 956-974. https://doi.org/10.1016/j.sandf.2012.11.014.

[11]. Mitchell JK, Baxter CD, Munson TC. Performance of improved ground during earthquakes. In Soil improvement for earthquake hazard mitigation 1995;1-36.

[12]. Seed RB, Cetin KO, Moss RES, Kammerer AM, Wu J, Pestana JM, Reimer MF. Recent advances in soil liquefaction engineering and seismic site response evaluation 2001.

[13]. Zeybek A, Madabhushi SPG. Influence of air injection on the liquefaction-induced deformation mechanisms beneath shallow foundations. Soil Dynamics and Earthquake Engineering 2017; 97:266-276. https://doi.org/10.1016/j.soildyn.2017.03.018.

[14]. Yegian MK, Eseller-Bayat E, Alshawabkeh A, Ali S. Induced partial saturation (IPS) for liquefaction mitigation: experimental investigation. J Geotech Geoenviron Eng, ASCE 2007; 133(4):372–80. https://doi.org/10.1061/(ASCE)1090-0241(2007)133:4(372).

[15]. Takemura J, Igarashi R, Izawa J, Okamura M. Centrifuge Model tests on soil desaturation as a liquefaction countermeasure. In: Proceedings of the 5th International conference on urban earthquake engineering, Tokyo institute of technology. Tokyo, Japan; 2008; 269–274.

[16]. Eseller-Bayat E, Yegian MK, Alshawabkeh A, Gokyer S. Liquefaction response of partially saturated sands. I: experimental results. J Geotech Geoenviron Eng, ASCE 2013; 139(6):863–871. https://doi.org/10.1061/(ASCE)GT.1943-5606.0000815.

[17]. He J, Chue J, Ivanov V. Mitigation of liquefaction of saturated sand using biogas. Géotechnique 2013; 63(4):267–275. http://dx.doi.org/10.1680/geot.SIP13.P.004.

[18]. Tokimatsu K, Yoshimi Y, Ariizumi K. Evaluation of liquefaction resistance of sand improved by deep vibratory compactions. Soils Found 1990;30(3):153–158. https://doi.org/10.3208/sandf1972.30.3_153.

548 [19]. Okamura M, Ishihara M, Oshita T. Liquefaction resistance of sand deposit improved with sand
549 compaction piles. Soils Found 2003; 43(5):175–187. https://doi.org/10.3208/sandf.43.5_175.
550 [20]. Yoshimi Y, Yanaka K, Tokimatsu K. Liquefaction resistance of a partially saturated sand. Soils
551 Found 1989; 29(2):157–162. https://doi.org/10.3208/sandf1972.29.3_157.
552 [21]. Okamura M, Soga Y. Effects of pore fluid compressibility on liquefaction resistance of partially
553 saturated sand. Soils Found 2006; 46(5):695–700. https://doi.org/10.3208/sandf.46.695.
554 [22]. Takemura J, Kondoh M, Esaki T, Kouda M, Kusakabe O. Centrifuge model tests on double
555 propped wall excavation in soft clay. Soils and Foundations 1999; 39(3):75-87.
556 https://doi.org/10.3208/sandf.39.3_75.
557 [23]. Schofield AN. Dynamic and earthquake geotechnical centrifuge modelling. In: Proceedings of
558 International conference on recent advances in geotechnical earthquake engineering and soil
559 dynamics, University of Missouri-Rolla. MO, USA 1981;1081–1100.
560 [24]. Kutter BL. Effects of capillary number, Bond number, and gas solubility on water saturation of
561 sand specimens. Can Geotech J 2013; 50(2):133–144. https://doi.org/10.1139/cgj-2011-0250.
562 [25]. Atkinson, J. The mechanics of soils and foundations. CRC Press 2007.
563 [26]. Kayen RE, Mitchell JK. Assessment of liquefaction potential during earthquakes by Arias
564 intensity. Journal of Geotechnical and Geoenvironmental Engineering 1997; 123(12):1162-1174.
565 https://doi.org/10.1061/(ASCE)1090-0241(1997)123:12(1162).
566 [27]. Dashti S, Bray JD, Pestana JM, Riemer MR. Wilson D. Centrifuge testing to evaluate and
567 mitigate liquefaction induced building settlement mechanisms. J. Geotech. Geoenviron. Eng.
568 2010 (a); 136(7):918–929. https://doi.org/10.1061/(ASCE)GT.1943-5606.0000306.
569 [28]. Bishop AW, Blight GE. Some aspects of effective stress in saturated and partly saturated soils.
570 Geotechnique 1963; 13(3):177-197. https://doi.org/10.1680/geot.1963.13.3.177.
571 [29]. Marasini NP, Okamura M. Numerical simulation of centrifuge tests to evaluate the performance
572 of desaturation by air injection on liquefiable foundation soil of light structures. Soils and

573 Foundations 2015; 55(6):1388-1399. https://doi.org/10.1016/j.sandf.2015.10.005.
574 [30]. Unno T, Kazama M, Uzuoka R, Sento N. Liquefaction of unsaturated sand considering the pore
575 air pressure and volume compressibility of the soil particle skeleton. Soils and Foundations 2008;
576 48(1):87-99. https://doi.org/10.3208/sandf.48.87.
577 [31]. Van Genuchten MT. A closed-form equation for predicting the hydraulic conductivity of
578 unsaturated soils 1. Soil science society of America journal 1980; 44(5):892-898.
579 [32]. Wang B, Zen K, Chen GQ, Zhang YB, Kasama K. Excess pore pressure dissipation and
580 solidification after liquefaction of saturated sand deposits. Soil Dynamics and Earthquake
581 Engineering 2013, 49:157-164. https://doi.org/10.1016/j.soildyn.2013.02.018.
582 [33]. Fredlund DG, Rahardjo H, Rahardjo H. Soil mechanics for unsaturated soils. John Wiley & Sons
583 1993.
584 [34]. Karamitros DK, Bouckovalas GD, Chaloulos YK. Insight into the seismic liquefaction
585 performance of shallow foundations. J. Geotech. Geoenviron. Eng. 2013; 139(4):599–607.
586 https://doi.org/10.1061/(ASCE)GT.1943-5606.0000797.
587 [35]. Sancio R, Bray JD, Durgunoglu T, Onalp A. Performance of buildings over liquefiable ground
588 in Adapazari, Turkey. Proc., 13th World Conf. on Earthquake Engineering, Canadian Association
589 for Earthquake Engineering, Ottawa 2004.
590 [36]. Zeybek, A., Madabhushi, S. P. G. Centrifuge testing to evaluate the liquefaction response of air-
591 injected partially saturated soils beneath shallow foundations. Bulletin of Earthquake
592 Engineering, 2017; 15(1):339-356.
593 [37]. Borcherdt RD. Estimates of site-dependent response spectra for design (methodology and
594 justification). Earthquake spectra 1994; 10(4):617-653. https://doi.org/10.1193/1.1585791.
595 [38]. Hardin BO, Drnevich VP. Shear modulus and damping in soils: design equations and curves.
596 Journal of Soil Mechanics & Foundations Div 1972;98(7).
597 [39]. Arulanandan K, Scott RF. Verification of numerical procedures for the analysis of soil

liquefaction problems. In International Conference on the Verification of Numerical Procedures for the Analysis of Soil Liquefaction Problems 1993.

[40]. Zeghal M, Elgamal AW, Zeng X, Arulmoli K. Mechanism of liquefaction response in sand–silt dynamic centrifuge tests. Soil Dynamics and Earthquake Engineering 1999; 18(1):71-85. https://doi.org/10.1016/S0267-7261(98)00029-3.

[41]. Adalier K, Elgamal AW. Seismic response of adjacent dense and loose saturated sand columns. Soil Dynamics and Earthquake Engineering 2002; 22(2):115-127. https://doi.org/10.1016/S0267-7261(01)00059-8.

[42]. Brennan AJ, Thusyanthan NI, Madabhushi SP. Evaluation of shear modulus and damping in dynamic centrifuge tests. Journal of Geotechnical and Geoenvironmental Engineering 2005; 131(12):1488-1497. https://doi.org/10.1061/(ASCE)1090-0241(2005)131:12(1488).

610 **Tables**

611

612 **Table 1** Index properties of Toyoura sand

Property	Value
Specific gravity, G_s	2.65
D_{50} (mm)	0.19
D_{10} (mm)	0.14
Maximum void ratio, e_{max}	0.973
Minimum void ratio, e_{min}	0.609
Void ratio @ D_r = 50%	0.791
Permeability, *k (m/s)*	2 x 10^{-4}
Relative density, D_r	50 %
Sand	100 %

613

614 **Table 2** Properties of foundation-structure system

Property	Foundation and superstructure*	
	Buffer Tank	Flare Stack
Footing dimension	4 x 4 x 1 m^3	4 x 4 x 2 m^3
Material used	Aluminum	Aluminum
Mass of footing	44.8 ton	87.04 ton
Thickness of superstructure	6 cm	6 cm
Outer diameter of superstructure	1.6 m	1.6 m
Height of lumped mass	7.6 m	14 m
Lumped mass	28.16 ton	14.08 ton
Bearing pressure @ 40g	51.2 kPa	71.2 kPa
Design period of soil-structure system	0.4 s (2.5 Hz)	0.5 s (2 Hz)

*All units are given in prototype scale

615

Table 3 Distribution of different transducers within the model ground

Level	Transducers*	Location (prototype scale)		Initial effective stress (σ'_{vo})		
		X m	Z (depth) m	Magnitude, kPa (prototype scale) Fully saturated**	Partially saturated***	Description
Level 1	P1, A1	12	10	91.60	93.56	Model centerline
Level 2	A2	12	8	63.12	65.08	Model centerline
Level 3	P2	18	6	50.42	52.38	Below FS footing
	P3, A3	12	6	51.64	53.60	Model centerline
	P4	6	6	46.72	48.68	Below BT footing
Level 4	P5	18	4	43.69	45.65	Below FS footing
	A4	12	4	31.16	33.12	Model centerline
	P6	6	4	36.69	38.65	Below BT footing
Level 5	P7	18	2	43.00	44.96	Below FS footing
	P8, A5	12	2	08.36	10.32	Model centerline
	P9	6	2	31.00	32.96	Below BT footing

*A: acceleration transducers, P: pore pressure transducers

**Water table in case of fully saturated model ground is 0.7 m (17.5 mm in model scale) below the top surface of model ground

***Water table in case of partially saturated model ground is 0.9 m (22.5 mm in model scale) below the top surface of model ground

Table 4 Test conditions and properties of applied main shakings

Model description	Test conditions		Peak acceleration of input ground motion (m/s^2) in prototype scale	
	Relative density D_r (%)	Degree of saturation S_r (%)	Tokachi-Oki ground motion*	Tohoku ground motion**
Fully saturated model ground	53.1	99.1	1.51	7.1
Partially saturated model ground	51.8	88.4	1.7	7.3

*Ground motion recorded at Hachinohe Port (NS component) during the 1968 Tokachi-Oki earthquake

**Design earthquake motion for highway bridges in Japan (2-I-I-3, NS component) recorded at the ground surface near the New Bansuikyo Bridge, Tochigi during 2011 Tohoku earthquake

626 **Figures**

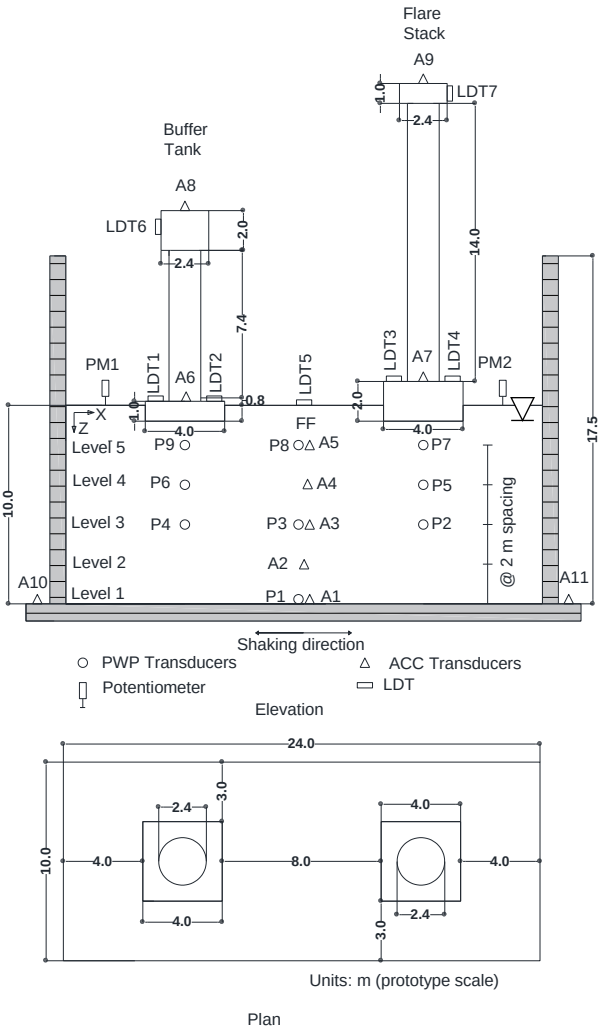

627

628 **Fig. 1**. Centrifuge model layout

629

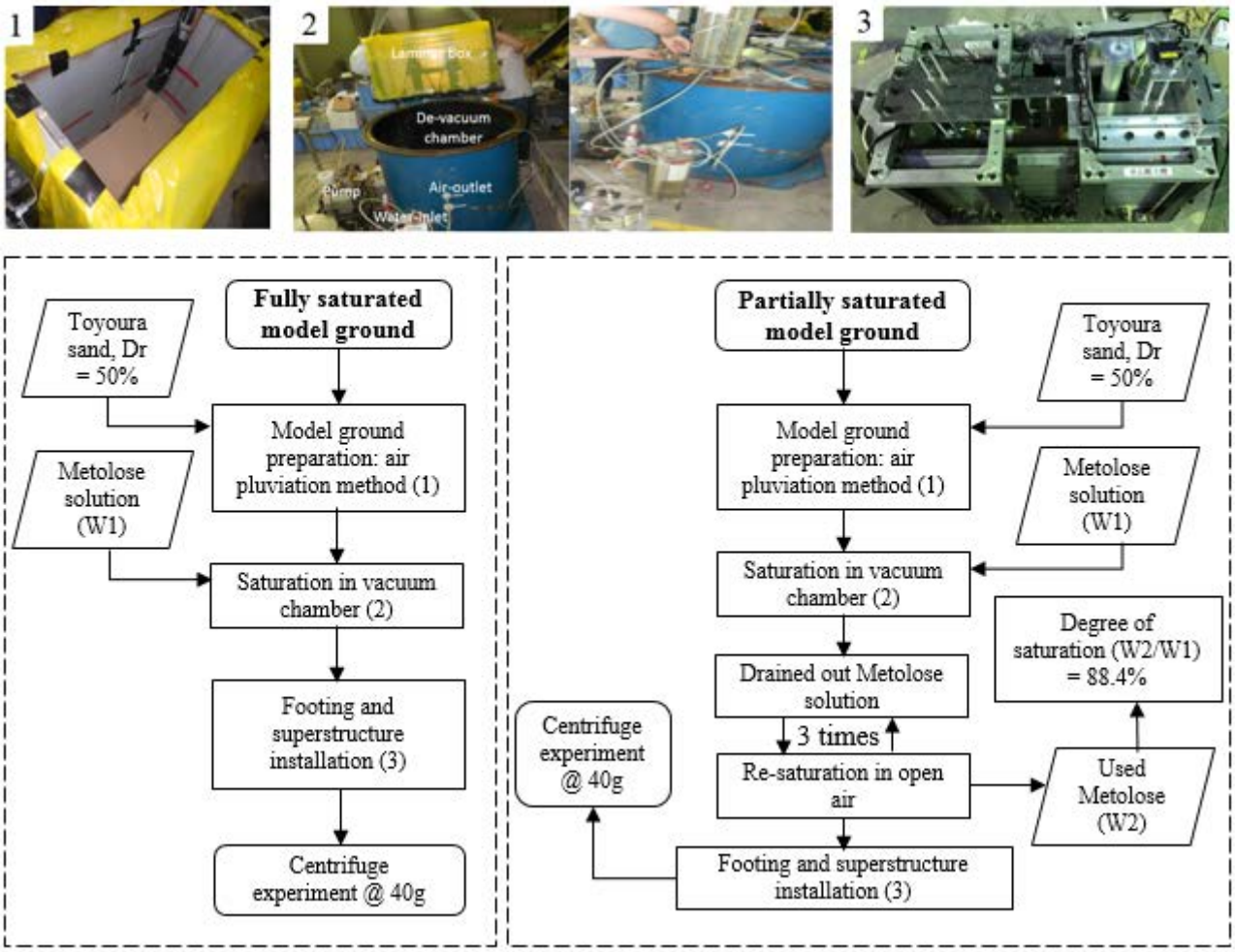

Fig. 2. Flow chart for fully saturated and partially saturated model ground preparation

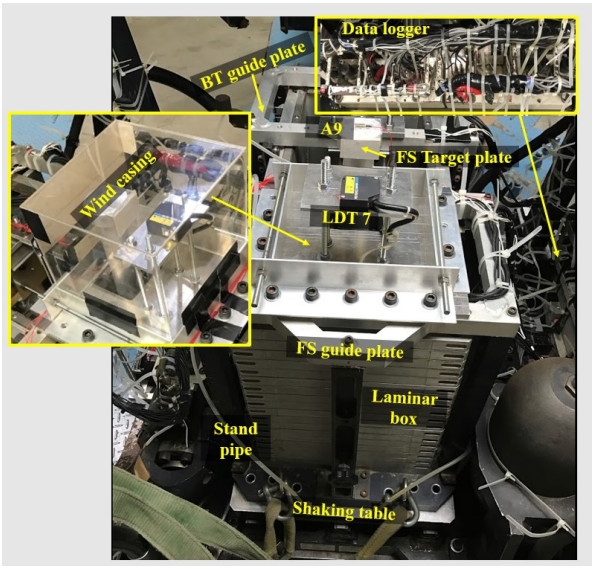

Fig. 3. Instrumented model setup mounted on centrifuge shaking table

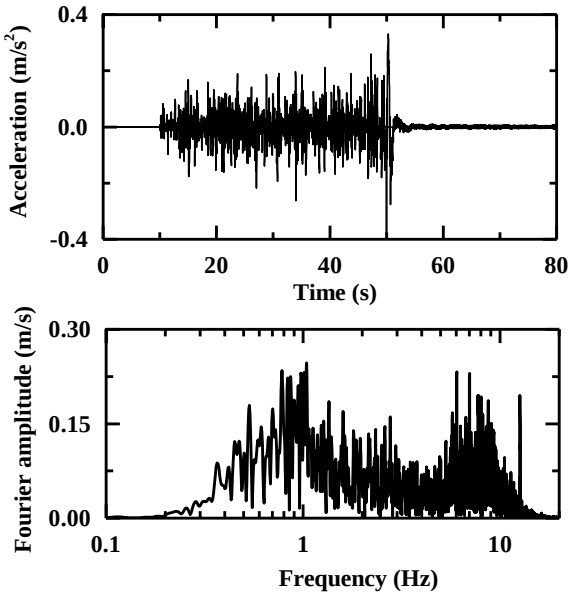

636

637 **Fig. 4.** Acceleration time history and Fourier spectra of input white noise (WN1) in prototype scale

638

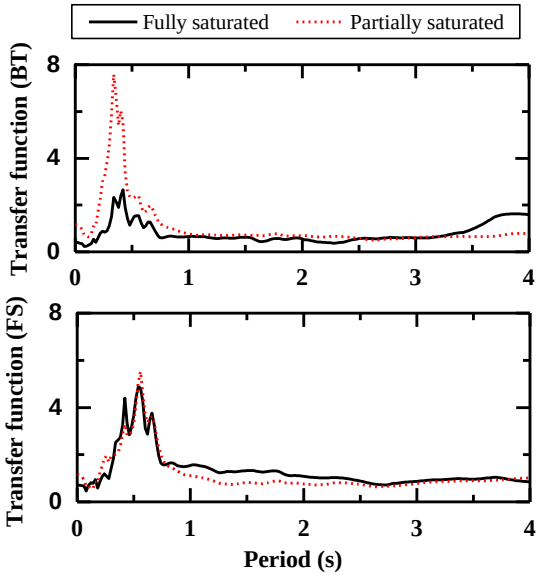

639

640 **Fig. 5.** Transfer Function obtained at top of Buffer Tank and Flare Stack in prototype scale

641

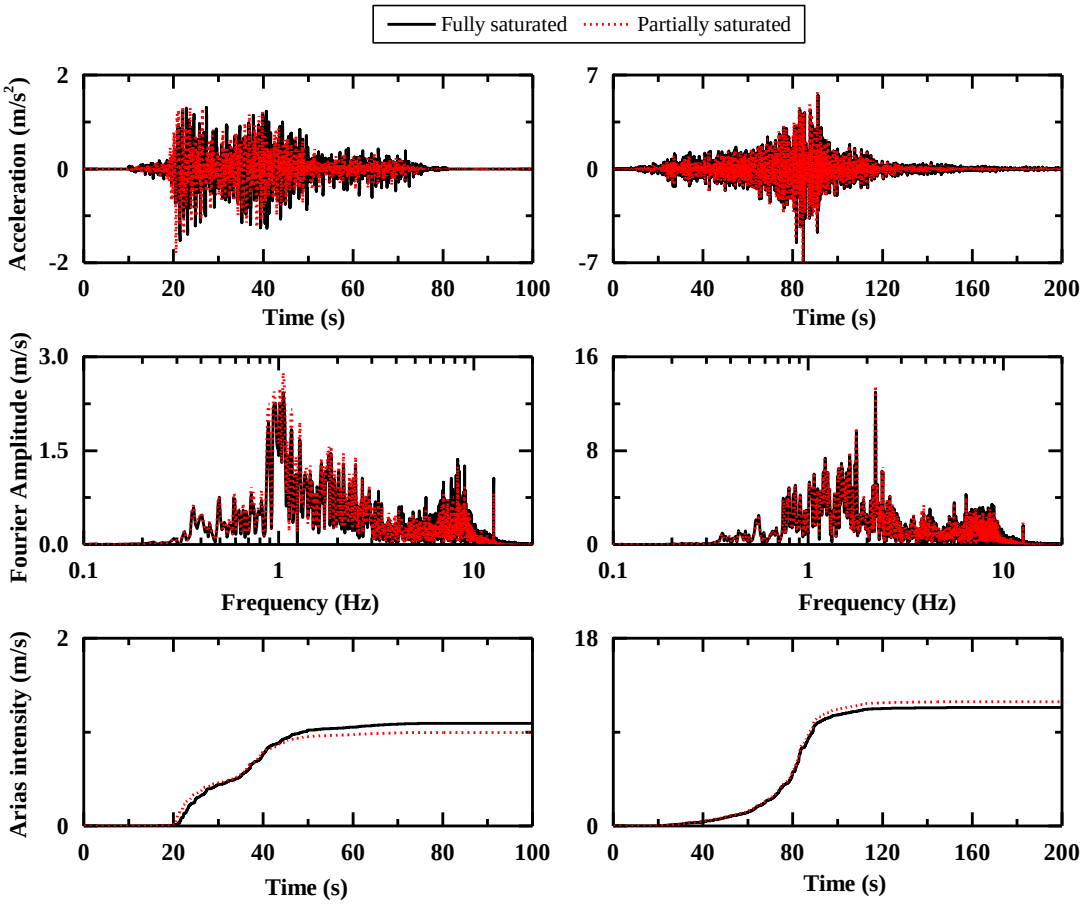

642

643 **Fig. 6.** Acceleration time histories, Fourier spectra and Arias intensities of Tokachi-Oki (left) and
644 Tohoku (right) ground motions for both fully and partially saturated model grounds in prototype scale
645

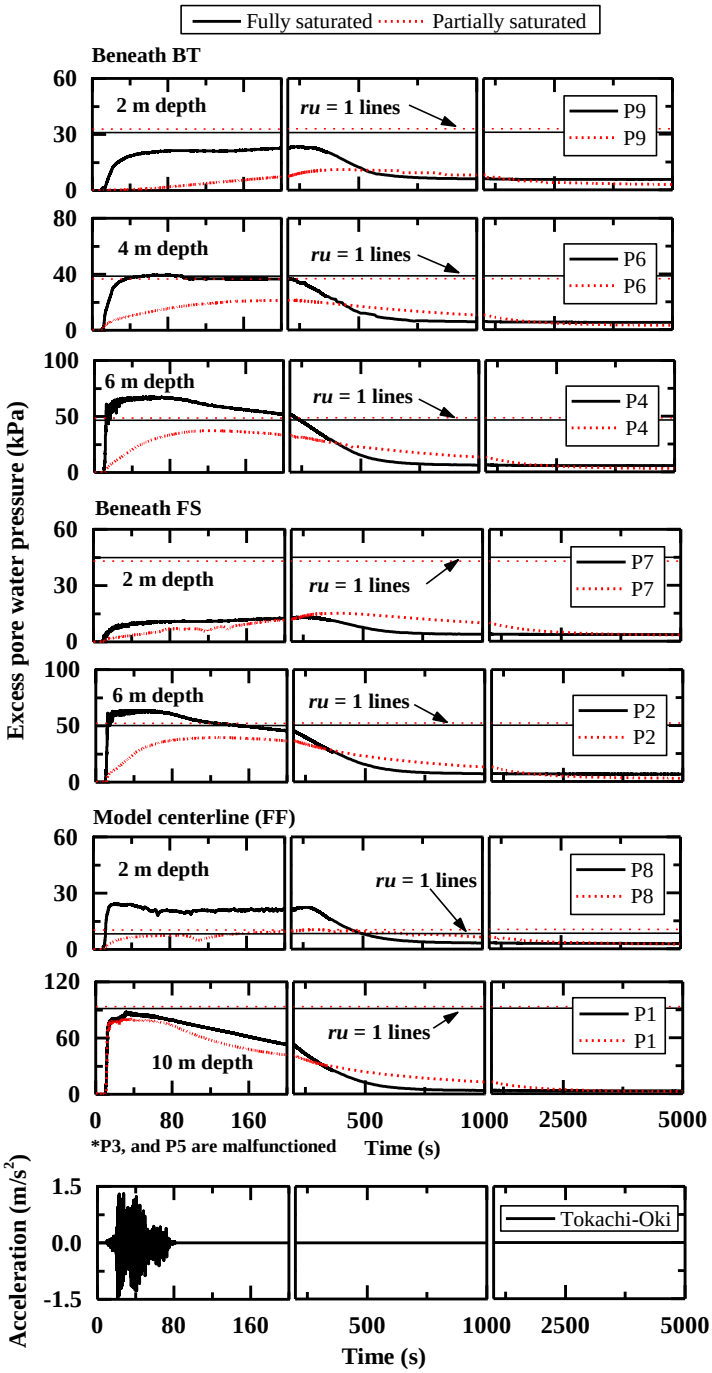

Fig. 7. EPWP time histories obtained during Tokachi-Oki ground motion

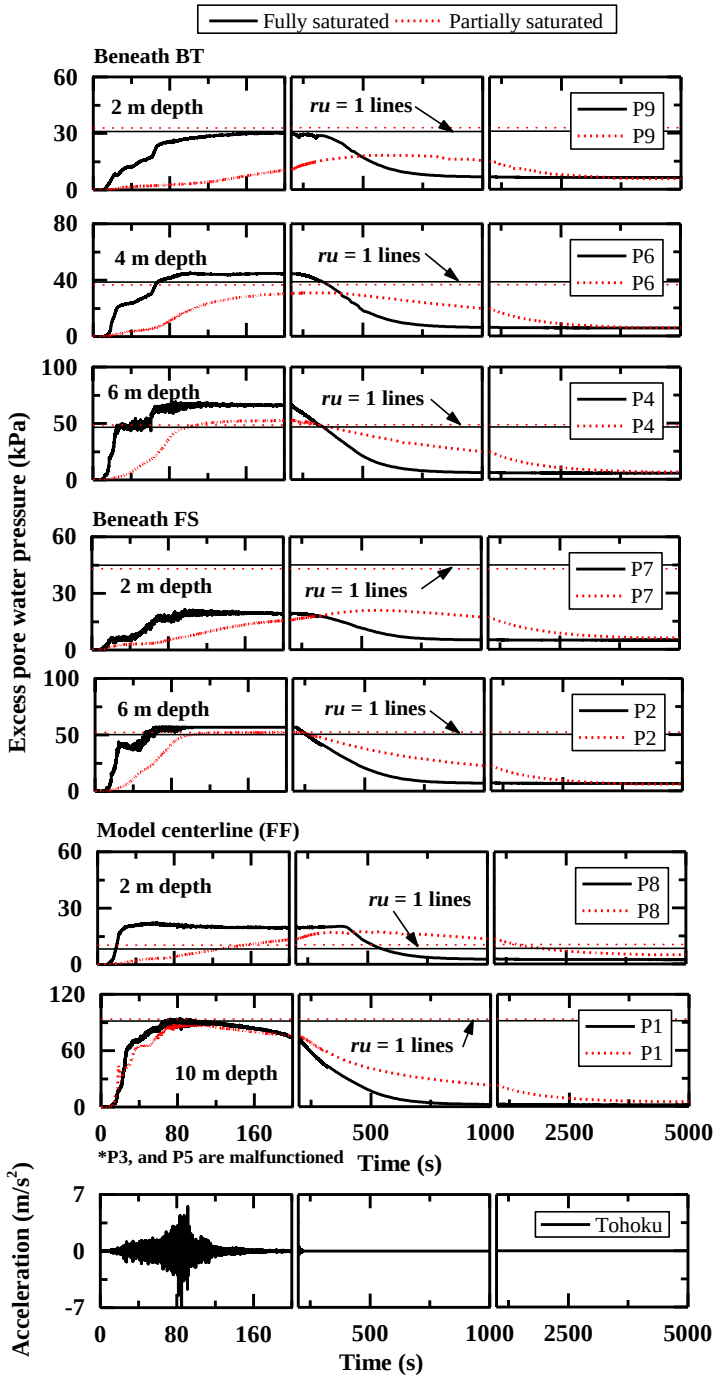

649

650 **Fig. 8.** EPWP time histories obtained during Tohoku ground motion

651

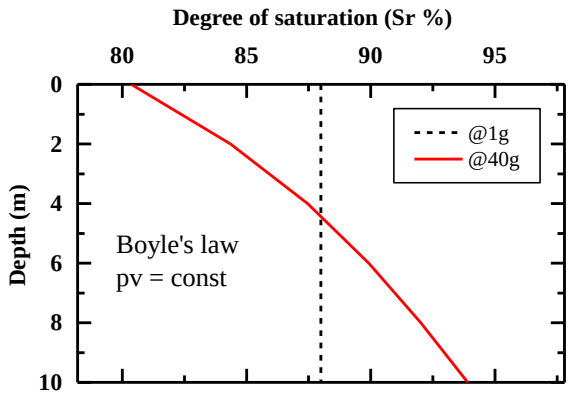

652

653 **Fig. 9.** Variation of degree of saturation within the partially saturated model ground

654

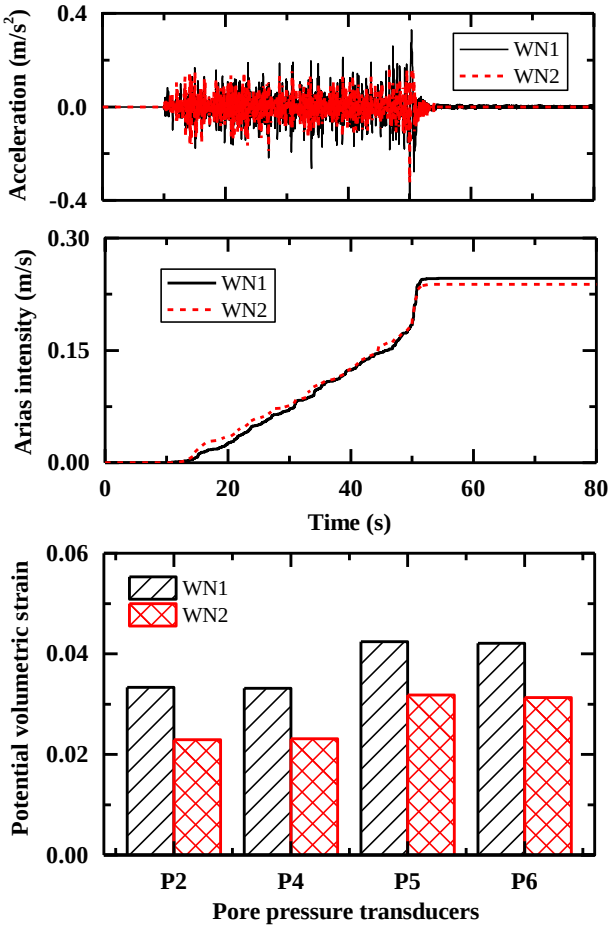

655

656 **Fig. 10**. Maximum potential volumetric strain during white noise 1 (WN1) and white noise 2 (WN2)

657

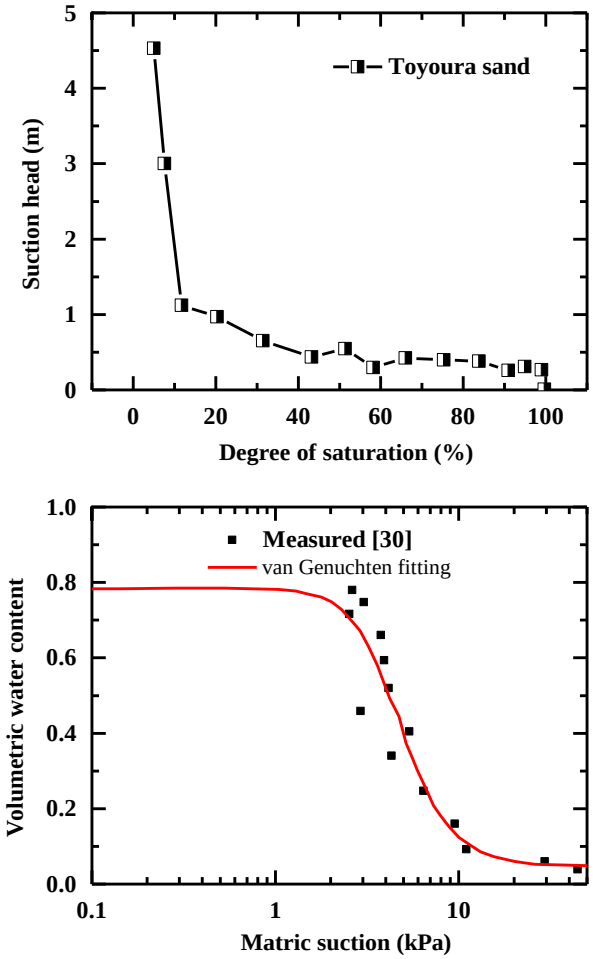

Fig. 11. Soil-water characteristic curve for Toyoura sand (after Unno et al. [30])

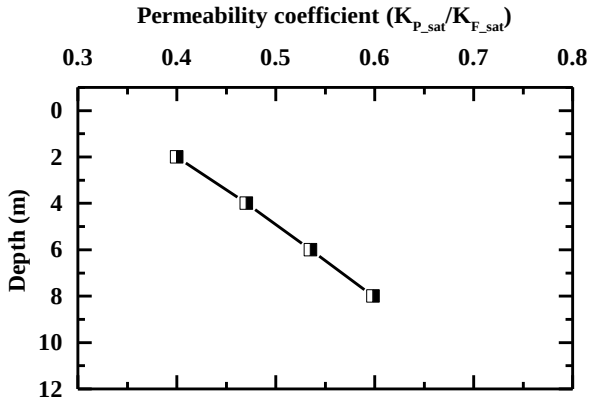

Fig. 12. Change in permeability because of induced partial saturation

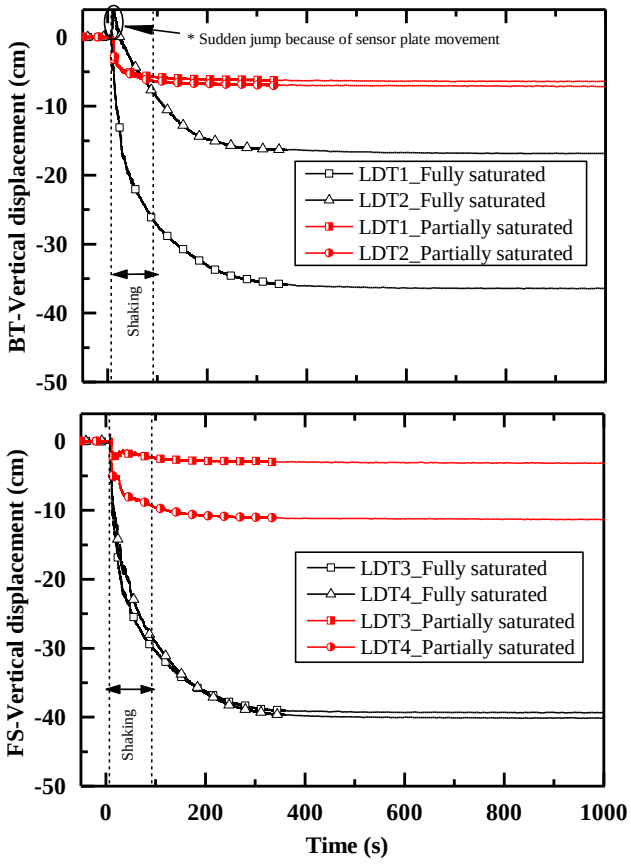

664

665 **Fig.13.** Settlement time histories of BT (LDTs 1 and 2) and FS (LDTs 3 and 4) during Tokachi-Oki

666 ground motion

667

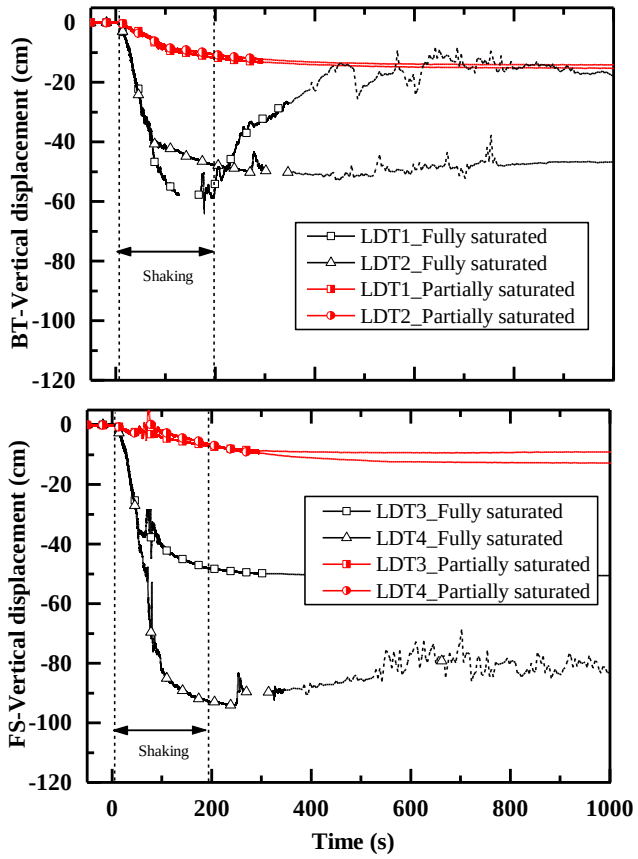

668

669 **Fig. 14.** Settlement time histories of BT (LDTs 1 and 2) and FS (LDTs 3 and 4) during Tohoku ground

670 motion

671

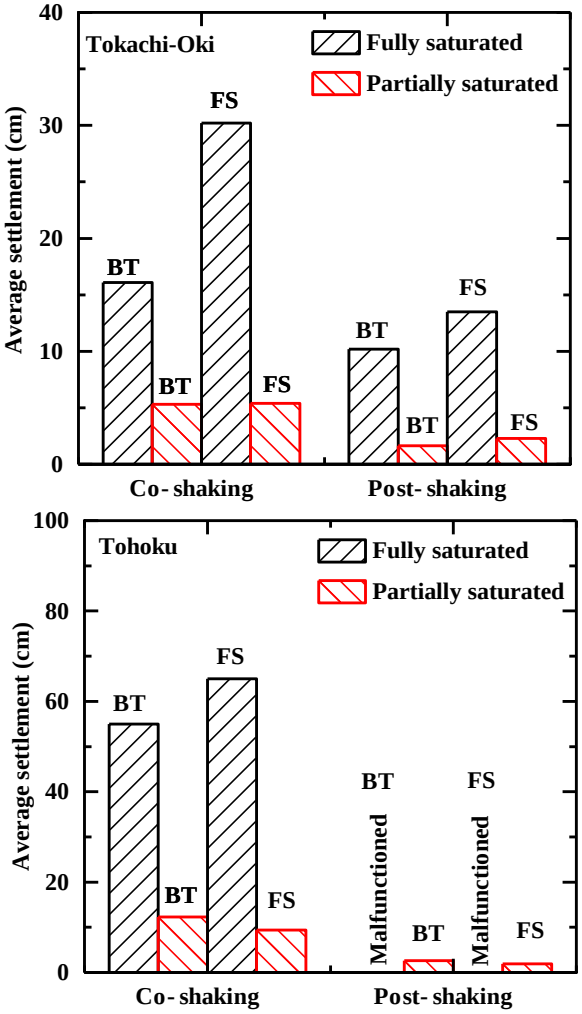

672

673 **Fig. 15.** Co-shaking and post-shaking settlement during Tokachi-Oki and Tohoku ground motion

674

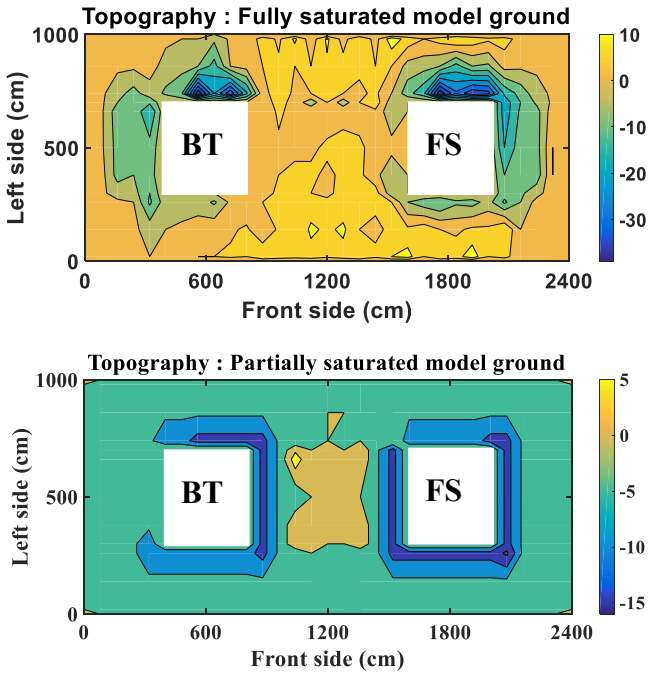

675

676 **Fig. 16.** Topography (surface settlement in cm) after the centrifuge experiment

677

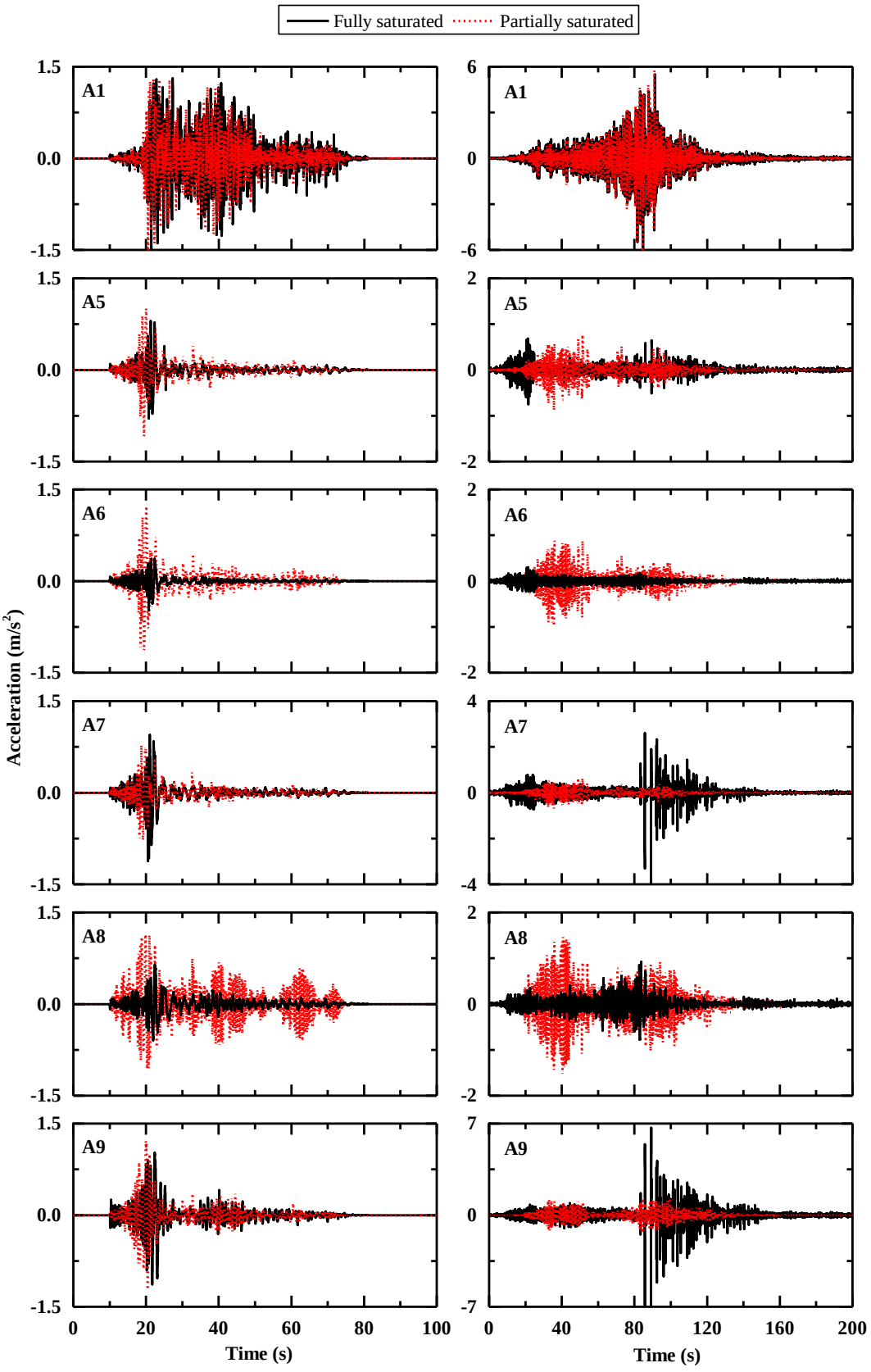

678

679 **Fig. 17.** Acceleration time histories during Tokachi-Oki (left) and Tohoku (right) ground motions

680

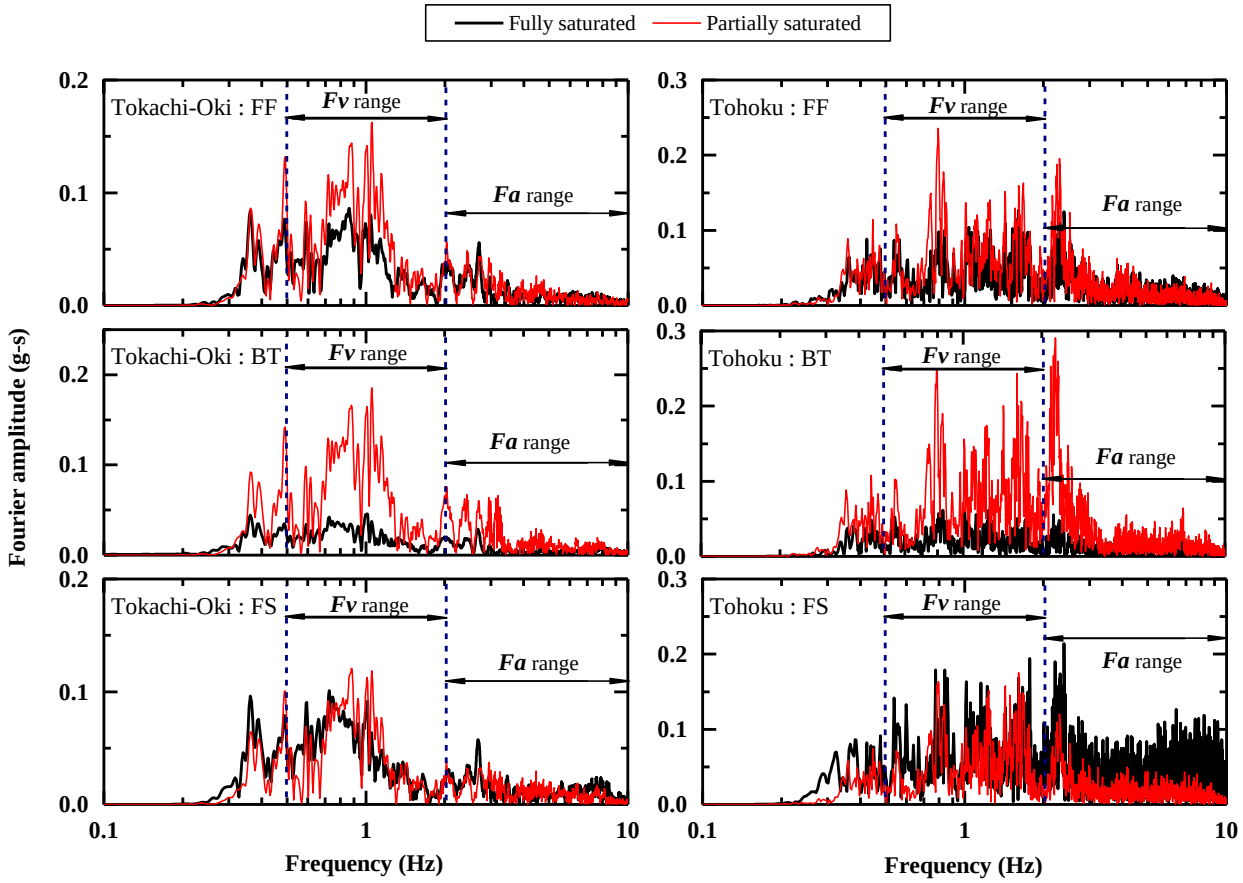

Fig. 18. Fourier amplitude spectra of acceleration recorded at footings of BT and FS and free field

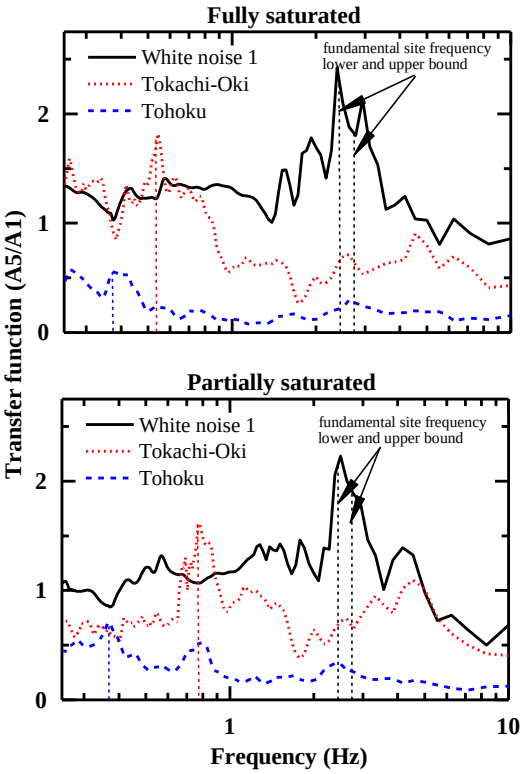

684

685 **Fig. 19.** Far-field model ground behavior during white noise, Tokachi-Oki, and Tohoku ground motions

686

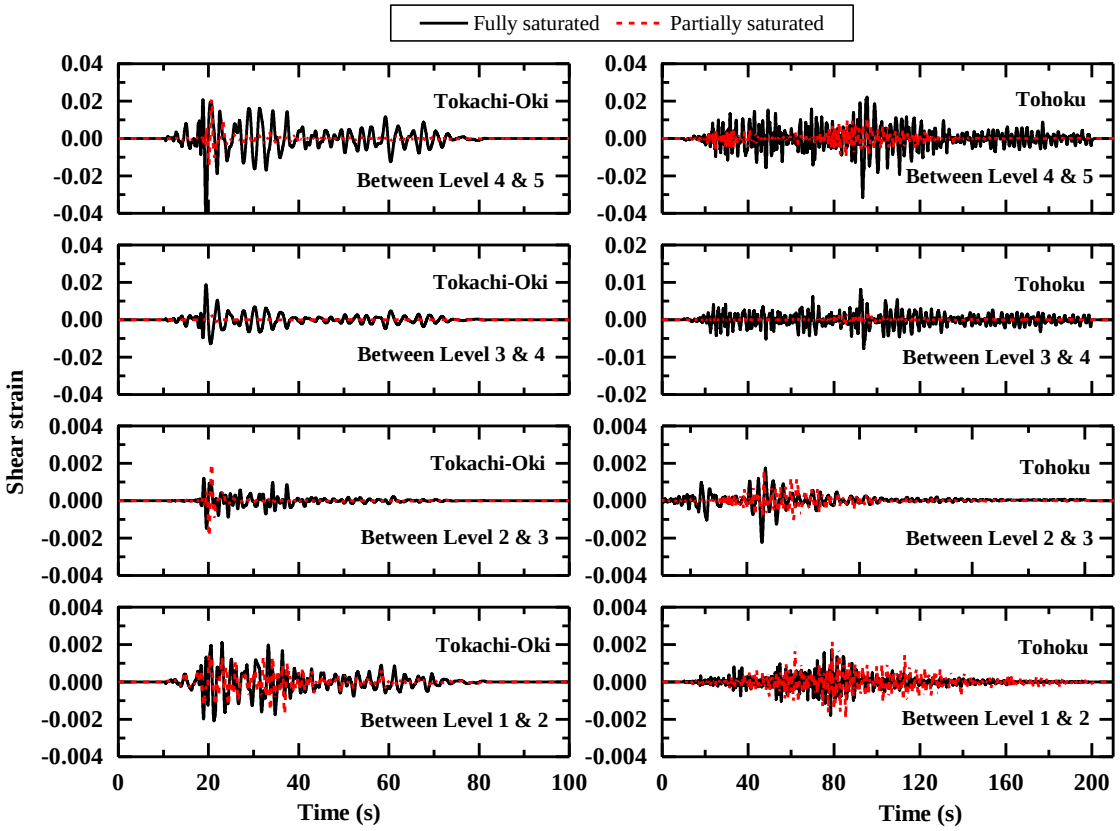

687

688 **Fig. 20.** Shear strain time histories along model centerline (MC) between different levels